Development of an Automatic Linear Calibration Method for High Resolution Single Particle Mass Spectrometry: Improved Chemical Species Identification for Atmospheric Aerosols

Authors: Shengqiang Zhu[1], Lei Li[2], Shurong Wang[1], Mei Li[2], Yaxi Liu[1], Xiaohui Lu[1], Hong Chen[1], Lin Wang[1, 3], Jianmin Chen[1, 3], Zhou Zhen[2], Xin Yang*[1, 3, 4] and Xiaofei Wang*[1, 3]

[1]*Shanghai Key Laboratory of Atmospheric Particle Pollution and Prevention, Department of Environmental Science and Engineering, Fudan University, Shanghai 200433, China*

[2]*Institute of Mass Spectrometer and Atmospheric Environment, Jinan University, Guangzhou, 510632, China*

[3]*Shanghai Institute of Pollution Control and Ecological Security, Shanghai 200092, China*

[4]*School of Environmental Science and Engineering, Southern University of Science and Technology, Shenzhen 518055, China*

Atmospheric Measurement Techniques

June 3rd, 2020

*To whom correspondence should be addressed.

Correspondence to:
Xiaofei Wang
Email: xiaofeiwang@fudan.edu.cn Tel: +86-21-31242526
Xin Yang
Email: yangxin@fudan.edu.cn Tel: +86-21-31245272

Abstract

The mass resolution of laser desorption ionization (LDI) single particle aerosol mass spectrometry (SPAMS) is usually low (~500), which has been greatly improved by recent development of delayed ion extraction technique. However, due to large fluctuations among LDI processes during each laser shot, accurate calibration of mass-to-charge ratio for high resolution SPAMS spectra is challenging. Here we developed an automatic linear calibration method to improve the accuracy of mass-to-charge (m/z) measurement for single atmospheric aerosol particles. Laboratory generated sea spray aerosol and atmospheric ambient aerosol were tested. After the calibration, the fluctuation ranges of the reference ions (e.g. Pb^+ and SO_4^+) m/z reaches ±0.018 for sea spray aerosol and ± 0.024 for ambient aerosol in average mass spectra. With such m/z accuracy, the HR-SPAMS spectra of sea spray aerosol can easily identify elemental compositions of organic peaks, such as C_x, C_xH_y and $C_xH_yO_z$. While the chemical compositions of ambient aerosols are more complicated, C_xH_y, $C_xH_yO_z$ and CNO peaks can also be identified based on their accurate mass. With the improved resolution, the time series of peaks with small m/z differences can be separated and measured. In addition, it is also found that applying high resolution data with enhanced mass calibration can significantly affect particle classification (identification) using the ART-2a algorism, which classify particles based on similarities among single particle mass spectra.

1. Introduction

Atmospheric aerosols can significantly impact radiative forcing, cloud formation and human health(Ackerman et al., 2004; Zhang and Kin-Fai, 2012). They originate from various sources and undergo many atmospheric aging processes, resulting in an extremely complicated mixture of particles with a large range of sizes and chemical compositions. This mixture is usually referred as “mixing state”. Measurement of aerosol mixing state requires single particle characterization techniques. Utilizing laser ablation/ionization of singe aerosol particle, Single Particle Aerosol Mass Spectrometer (SPAMS) has been widely used to measure chemical compositions, sizes and refractory index of aerosols in real-time(Moffet and Prather, 2009; Murphy, 2010; Sullivan and Prather, 2005). Based on this technique, ART-2a and other algorithms had been developed to classify the ambient particles based on their mass spectra and identify their sources (Reinard et al., 2007; Zelenyuk and Imre, 2009).

However, SPAMS with laser desorption/ ionization (LDI) method has several serious limitations (Manuel et al., 2006; Wenzel et al., 2003). A major issue is that the mass resolution of the SPAMS is relatively low (~500) and the accuracy of m/z (mass to charge ratio) is usually at integer level, resulting in uncertainties about the identification of chemical species (Nash et al., 2006; Pratt and Prather, 2012; Qin et al., 2006). Due to the low mass resolution, many organic and inorganic peaks cannot be separated, such as K^+ /$C_3H_3^+$ from the m/z peak of 39, Al^+ $C_2H_3^+$ from the m/z peak of 27 and CN^- /$C_2H_2^-$ from the m/z peak of -26 (Li et al., 2018). To better identify these particulate chemical species, A higher mass resolution version of the SPAMS with better m/z accuracy is needed.

Recently, Li et al., significantly increased SPAMS’s mass resolution to ~2000 by applying delayed ion extraction technique, which combined a standard rectangular extraction pulse with an exponential pulse (Li et al., 2018). This new SPAMS is called high resolution (HR)-SPAMS. Unfortunately, in spite of resolution enhancement with this new technique, ion

peak position was still very sensitive to initial ion coordinate and speed. Chudinov et al., has demonstrated that the ion peak shifts of 208[Pb^+] and 147[$Na(NO_3)_2^-$] could be varied in the range of ±10 ns and the ion start position could be varied in the range of ±150μm. As a result, substantial peak jittering is observed when switching between mass spectra of each individual particle. This peak jittering leads to a fact that isotopic pattern identification becomes more difficult by averaged mass spectrum(Chudinov et al., 2019). Furthermore, the peak jittering is different in each single particle mass spectrum. In other words, the calibration parameter for each mass spectrum should be significantly different and calibration is required for each particle. Therefore, in order to get accurate m/z, Chudinov et al. used several peaks with known m/z to calibrate every SPAMS spectrum for $Pb(NO_3)_2$ and NaI particles produced from an atomizer.

In this study, we report a calibration method for single particle high resolution mass spectra data. Based on the assumption that the sea spray aerosol has relatively simple chemical composition while the ambient aerosol has more complex chemical composition, the performance of the calibration method had been evaluated in detail for these two aerosol systems with different complexity. In addition, the impact of using high resolution SPAMS data on particle classification by ART-2a algorithm was assessed. An open source code specific for HR-SPAMS was made and we proposed the principle of this calibration method can be applied into some similar instruments, such as single particle mode Aerosol Mass Spectrometer (AMS).

However, atmospheric particles are extremely complicated with a wide range of chemical compositions and sizes (Zhang et al., 2013), which brings much greater challenge to properly calibrating each SPAMS mass spectra and obtaining accurate m/z measurement. We need to develop a new MS calibration method for atmospheric aerosols and evaluate its performance comprehensively.

2. Experimental Section

2.1 High Resolution Single Particle Aerosol Mass Spectrometer (HR-SPAMS)

The detailed description of HR-SPAMS (Hexin Analytical Instrument Co., Ltd., China) can be found elsewhere(Li et al., 2018). Briefly, a HR-SPAMS consists of an aerodynamic lens as its particle inlet, two laser beams system for particle sizing, a UV laser for LDI and a bipolar time-of-flight mass analyzer for the detection of positive and negative ions. Positive and negative ions are detected by two z-shape bipolar TOF reflectron mass analyzers. The size detection range of HR-SPAMS is 200-2000 nm. As introduced before, this HR-SPAMS used delayed ion extraction technique to enhance its mass resolution.

2.2 Laboratory generated sea spray aerosol

Sea spray aerosol was produced by water jet method. In a sea spray aerosol production tank, a seawater jet was hitting seawater surface and producing bubbles, which would rise to the surface and burst. Bubble bursting process produces sea spray aerosols. Seawater was collected at Fengxian, Shanghai (30°92'N and 121°47'E) on March 30st (Fig.S1).

2.3 Ambient aerosol sampling

Ambient aerosol sampling was conducted at Fudan university, Shanghai (31°20'N and 121°30'E) on May 29th 2019 (Fig.S1). The ambient particles were dried by a diffusional dryer before being sampled by the HR-SPAMS.

3. Development of Calibration Methods

3.1 Automatic linear calibration method

To improve the accuracy of m/z for HR-SPAMS spectra, an automatic linear calibration method has been developed. Noticeably, due to the technical limitation of data acquisition, the whole HR-SPAMS spectrum is not continuous but divided by a large number of m/z bins, which are described in Fig.S2(a partial enlarged detail in the single particle mass spectra) and can be viewed as the probability density histogram of the m/z. Here we denote "m/z bin value" as the median m/z value of each bin.

The linear calibration method is described as the following steps:

Step 0: The SPAMS data was coarsely-calibrated by the traditional method, which usually selected a few particles with distinct ion patterns, i.e. the molecular composition of some distinct peaks in the mass spectra can be easily identified. Then, the time of flight of these peaks and the true m/z of the corresponding ions were used to calculate a set of calibration parameters for positive and negative spectra. The parameters were finally applied to the whole mass spectra dataset, and coarsely-calibrated was completed.

Step 1: a pool of ion peaks in the single particle mass spectra were selected as the potential m/z calibration reference ions. The selection criteria are (1) these peaks should be present in most of the spectra; (2) the identification of these ion peaks should not be significantly affected by other adjacent peaks. For example, 27$[Al]^+$ was not selected, as its adjacent peak 27$[C_2H_3]$ may affect the peak shape and identification of 27[Al] .

According to the previous research, possible peak assignments for the m/z of reference ions for sea spray aerosol and ambient aerosol were listed on Table 1(Bertram et al., 2018; Collins et al., 2014; Tsunogai et al., 1972; Wang et al., 2016; Wang et al., 2019). For sea spray aerosol, according to several studies (Bertram et al., 2018; Collins et al., 2014; Tsunogai et al., 1972), the reference ions with m/z 23 24 39 -35 -37 were 23$[Na]^+$ 24$[Mg]^+$ 39$[K]^+$ -35$[Cl]^-$ and -37$[Cl]^-$ respectively. And Collins et al. shows that the reference ions with m/z 81, 83, -26, -42, -58, -129, and -131 were 81$[Na_2Cl]$, 83$[Na_2Cl]$, -26[CN] , -42$[CNO]^-$, -58$[NaCl]^-$, -129$[MgCl_3]^-$, and -131$[MgCl_3]^-$, respectively (Collins et al., 2014). Due to the fact that Na, Mg and K were abundant in sea spray aerosol, the reference ions with m/z 113 and 115 should be 113$[K_2Cl]^+$ and 115$[K_2Cl]^+$.Thus, in this study, we select 23$[Na]^+$, 24$[Mg]^+$, 39$[K]^+$, 81$[Na_2Cl]^+$, 83$[Na_2Cl]^+$, 113$[K_2Cl]^+$, 115$[K_2Cl]^+$, -35$[Cl]^-$, -37$[Cl]^-$, -26$[CN]^-$, -42$[CNO]^-$, -129$[MgCl_3]^-$, -131$[MgCl_3]^-$, -58$[NaCl]^-$ as the potential reference ions for sea spray aerosols.

For the ambient aerosol, according to the previous ambient SPAMS measurements(Wang et al., 2016; Wang et al., 2019), the reference ions with m/z 12, 23, 36, 39, 56, 207, 208, and 209 were assigned to 12$[C]^+$, 23$[Na]^+$, 36$[C_3]^+$, 39$[K]^+$, 56$[Fe]^+$, 207$[Pb]^+$, 208$[Pb]^+$

and 209[Pb]$^+$, the reference ions with m/z -26, -35, -46, -62, -96, and -97 were assigned to -26[CN]$^-$, -35[Cl]$^-$, -46[CNO]$^-$, -62[NO_2]$^-$, -96[SO_4]$^-$ and -97[HSO_4]$^-$ respectively. So in this study, we select the 12[C]+, 23[Na]$^+$, 39[K]$^+$, 36[C3]$^+$, 56[Fe]$^+$, 208[Pb]$^+$, 206[Pb]$^+$, 207[Pb]$^+$, -62[NO3]$^-$, -26[CN]$^-$, -35[Cl]$^-$, -96[SO4]$^-$, -46[NO2]$^-$, -97[HSO4]$^-$ as the potential reference ions for ambient aerosols.

Step 2: a set of reference ions was chosen from the potential reference ion pool for each spectrum. The selection was based on the absolute ion intensity of the reference ions in this spectrum. They must be greater than a threshold, e.g. we set 15 a.u. for ambient aerosol and 8 a.u. for sea spray aerosol, respectively. A particle was discarded from the spectra database if it did not have enough reference ions (the minimum number of reference ions was set to be 5) in either positive or negative mass spectrum.

Step 3: the reference ions were used to calibrate m/z for mass spectra of each particle. As introduced before, a HR-SPAMS spectrum consists of a number of bins. The measured m/z bin values of the reference ions mentioned in the Step0 were calibrated based on their theoretic (or true) m/z bin values. A linear regression between the two set of variables (measured vs. theoretic m/z bin values) was conducted, and two calibration parameters (a slope and an intersect) can be obtained. Then we used these parameters to make the calibration for every bin value in this mass spectra. Finally, the m/z of the whole spectrum had been corrected. Thus, we assigned a m/z bin value to each corrected m/z based on proximity principle. Finally, mass spectra with well calibrated bin value can be obtained for each single particle.

A GUI program for this automatic linear calibration method had been developed for the sake of easy use (Fig. 1). The MATLAB codes for this GUI and the automatic linear calibration method are open access and available at https://github.com/zhuxiaoqiang-fdu/zhuxiaoqiang-fdu.

3.2 Evaluation of the calibration method

In this study, a total of 5,130 sea spray aerosol particles and 5,007 ambient aerosol particles

were analyzed. And 4,624 sea spray particles and 1,409 ambient particles were successfully calibrated. As some fraction of particles had been filtered because their mass spectrum did not have 5 or more reference peaks to conduct the calibrations. To mitigate this problem, we proposed some adjustments in the next section. Figure 2 shows that the calibration curves for a random selected sea spray aerosol particle and ambient aerosol particle. The adj-R^2 coefficients of both calibration curves are equal to ~1, demonstrating that this calibration method is effective and accurate. All the slopes and intercepts of the linear calibration can be found in the Fig.S3 and Fig.S4. In addition, Figure 3a and 3b report a comparison of m/z distributions of reference ions between before and after automatic linear calibration. The results show that the fluctuations of the reference ions m/z were significantly reduced after automatic linear calibration. The average m/z deviation of the reference ions was reduced from ~0.04 to ~0.001 for sea spray aerosol, and from ~0.035 to ~0.006 for ambient aerosol, respectively.

3.3 Automatic linear calibration method with a larger reference ion pool

It is important to note that a large number of ambient particles were filtered because their spectra did not have 5 or more reference peaks to conduct calibrations. Especially, only ~29.0% of total ambient particles had sufficient number of reference ions in their positive spectra. To solve this problem, extra reference ions, including 67$[VO]^+$, 67$[C_5H_7]^+$, 89$[C_7H_5]^+$, 89$[Na_2BO_2]^+$, 102$[C_8H_6]^+$, 102$[CaNO_3]^+$, were added into the original positive reference ion pool. Obviously, these ions share the same integer m/z value with other ions. We needed to identify them using additional information other than their integer m/z values.

The specific reference ions was determined by their coarsely-calibrated m/z. Table S2 shows that the m/z deviation ranges of the reference positive ambient ions in coarsely-calibrated spectra before automatic linear calibration were around 0.011~0.048, while the m/z differences between 67$[VO]^+$ and 67$[C_5H_7]^+$, 89$[C_7H_5]^+$ and 89$[Na_2BO_2]^+$, 102$[C_8H_6]^+$ and 102$[CaNO_3]^+$ were 0.1213, 0.0622, and 0.083, respectively, which were larger than the m/z deviations of these reference ions in coarsely-calibrated spectra. Therefore, the coarsely-calibrated spectra can be used to determine these specific reference ions. With these additional potential reference ions, a total of 2490 ambient particles were calibrated,

much more than the previous analysis (1,409 ambient particles). The deviations from theoretical m/z for applying this expanded ion pool are summarized in Table S3. The average m/z deviation of the reference ions is ~0.0068.

4. Application to atmospheric aerosols measurement

4.1 HR-SPAMS measurement of sea spray aerosol

SPAMS data usually contains a large number of individual mass spectra. It is impossible to manually analyze every spectrum from a large dataset. Averaging a number of mass spectra is often preferred. However, to obtain averaged high-resolution spectrum, each spectrum must be well calibrated. Therefore, it would be very interesting to see what new information can be obtained from HR-SPAMS measurement of aerosols with the automatic calibration method. Figure 4 reports the average positive and negative mass spectra for the laboratory generated sea spray aerosols and the error limits mean the concluded accepted error range. Similar to the low-resolution sea spray aerosol mass spectra, they contain major peaks of Na^+, Mg^+, K^+, Na_2Cl^+, CN^-, Cl^-, CNO^-, $NaCl^-$, $NaCl_2^-$ and $MgCl_3^-$, as well as many smaller peaks, such as Ca^+, SiO_2^-/SiO_3^-, and KCl_2^-. With the improved m/z measurement, many peaks, which cannot be determined by integer resolution mass spectra, now can be clearly identified (Table 2). For example, the ion with m/z at 27.0267 is $C_2H_3^+$ rather than Al^+. The ion with m/z at 76.9336 is $CaCl^+$ rather than $C_6H_5^+$. And some sulfur containing organic ions, such as CS^+, can be determined. Surprisingly, we can identify the presence of HCO_2^- and $CaCO_3^-$, demonstrating that carbon hydrates are contained in sea spray aerosols.

4.2 HR-SPAMS measurement of atmospheric aerosol

Laboratory generated sea spray aerosol can be viewed as a relatively simple aerosol system, while the chemical compositions of ambient aerosols are much more complicated. Figure 5 shows the averaged HR-SPAMS mass spectra of the ambient aerosols sampled at Fudan University Jiangwan Campus on May 29th, 2019. With the improved m/z measurement, many organic ions, such as C_x, C_xH_y, and $C_xH_yO_z$ can be directly identified (Table 3). Also, we can separate the organic and inorganic species more directly with the high mass resolution. For instance, $C_6H_8^+$ can be clearly distinguished from possible interference of

Ca_2^-, TiO_2^+ and $NaKO^+$. $C_{10}H^-$ can also be identified from possible assignment of $NaSO_4^-$ etc. More importantly, 139[$C_2H_3O_5S^-$] (the theoretical m/z value: -138.97) can be clearly distinguished from other possible assignments, such as 139[$C_{11}H_7^-$] with the m/z value of -139.55 and 139[AsO_4^-] with the m/z value of -138.90. Moreover, 153[$C_3H_5O_5S^-$] with theoretical m/z value of -152.986 can be distinguished from other possible assignments, such as 153[$C_{12}H_9^-$] with m/z value of -153.070 and 153[$Na_2Cl_3^-$] with m/z value of -152.883. These two important organic ion peaks have been suggested to be the characteristic ion peaks for the organosulfates in secondary organic aerosols (Surratt et al., 2010; Surratt et al., 2007).

4.3 Time variation of HR-SPAMS measurement

With the high mass resolution of HR-SPAMS and enhanced m/z calibration, we were able to obtain an average mass spectrum from many particles. The accurate m/z values in the average mass spectrum can be used to separate peaks with close m/z and track their intensity variations. Here we conducted a time variation measurement for ambient aerosol from 11:00 on May 29th to 11:00 on May 30th2019. We selected first 500 particles collected by SPAMS during every hour for elemental analysis. Figure 6 shows that the peak at m/z 41 has a bimodal structure, whose m/z were at 40.9546 ± 0.0105 and 41.0194 ± 0.0105, respectively. Thus the peak with the smaller m/z is an isotope of K^+(theoretical m/z value of $^{41}K^+ = 40.96182$, theoretical m/z bin value of $^{41}K^+ = 40.9667$; this peak also follows the isotopic pattern of K) and the other peak should be $C_3H_5^+$(theoretical m/z value 41.03913, theoretical m/z bin value 41.03). Figure 6 shows that HR-SPAMS was able to separately measure the time series of these two peaks with a small m/z difference. In contrast, it is impossible for a low resolution (LR)-SPAMS to provide such detailed time variation measurement of these peaks.

4.4 Particle classification by ART-2a

Adaptive resonance theory neural network (ART-2a) is a widely-used method to classify particles based on the similarity among their mass spectra (Song et al., 1999). Here we make a comparison of ART-2a classification between the HR-SPAMS data and traditional

low resolution (LR)-SPAMS data. Particles with the positive and negative spectra were analyzed by ART-2a with a learning rate of 0.05, a vigilance factor of 0.7, and an iteration number of 20. The previous ambient aerosol SPAMS dataset (1,400 particles) was used for the matrix size of the ART-2a is around 7×10^7. The LR-SPAMS data, whose m/z was at integer level, was generated by summing high resolution SPAMS peaks in each integer m/z bin. The classification results show that the HR-SPAMS data was grouped to 93 categories and the top 45 categories accounted for 96 percent of all particles. The particle number of the first eight categories was 122, 101, 99, 86, 82, 70, 68 and 60 respectively. In contrast, the LR-SPAMS data was only grouped to 33 categories in total and the top 20 categories accounted for the 96 percent of all particles. The particle number of the first eight categories was 170, 118, 107, 107, 106, 92, 90 and 88 respectively. The detailed results can be found in the Fig.S5-S6. Obviously, ART-2a classification of high resolution SPAMS data generated more particle categories. This is mainly because HR-SPAMS mass spectra can differentiate peaks with close m/z, which may be viewed as one peak in LR-SPAMS data.

The ART-2a classification of the HR-SPAMS results (Fig.S6) show that the signal at 23[Na^+] in Type 2HR was stronger than Type 1HR while the signals at 26[CN^-] and 42[CNO^-] were weaker in Type1 HR. Meanwhile the averaged mass spectra of the Type 2HR showed the presence of 206[Pb^+], 207[Pb^+] and 208[Pb^+], which are known to be harmful to human health(Das et al., 2018; Peng et al., 2020). Furthermore, particles of Type 2HR containing abundant secondary inorganic components like [NO_2^-], [NO_3^-] and [SO_4^-], which originated from the aerosol aging processes (Dall'Osto and Harrison, 2012; Ma et al., 2016). In contrast, these two first particle types were lumped together into Type 1LR in the LR-SPAMS classification results (Fig.S5). Due to the merge of these two particle types, [Pb^+] ions were not significant. Meanwhile, Type 3,4,5HR classification results contain strong signals at 26[CN^-], 42[CNO^-], 46[NO_2^-], 62[NO_3^-] and 97[HSO_4^-], suggesting that these three types were from biomass burning or residential cooking burning. [K^+] is also another feature of this type particle emission (Bi et al., 2011; Hudson et al., 2004). There were obvious relative ion intensity differences at 26[CN^-], 42[CNO^-], 46[NO_2^-] and 62[NO_3^-] among these types, which implied that these three particle types

might be from different burning sources or experienced different levels of aging (Luo et al., 2020). While these three particle types were lumped together as Type 2LR. This critical information which could be potentially used to distinguish particle sources and aging processes was lost. Additionally, Type 7HR can be assigned as ECOC type, based on its strong signals at [C_x^+], [$C_xH_y^+$] and [$C_xH_yO_z^+$]. Particles of this type may come from the primary emission sources, and the emitted black carbon particles would also form this type particles after absorbing some low volatile organic compounds in the atmosphere (Sodeman et al., 2005). 97[HSO_4^-] can be observed to have a weaker signal than 62[NO_3^-] and 46[NO_2^-], which implied that the secondary reaction of SO_2 as the precursor of HSO_4^- was not significant in the particle surface for ECOC type particles in this study (SULLIVAN and PRATHER, 2007). In contrast, the classification results of the LR-SPAMS were not so clear and generated less particle types. Given HR-SPAMS spectra have much more detailed chemical information about particles, we would propose that the ART-2a classification of HR-SPAMS might be more accurate.

5. Conclusion

An automatic linear calibration method had been developed for data analysis of high-resolution SPAMS data. This technique can significantly improve the m/z accuracy of SPAMS spectra for atmospheric aerosol samples. The analysis of HR-SPAMS data for laboratory generated sea spray aerosols shows many details of its chemical compositions. For example, many organic ions, such as $C_2H_3^+$ and CS^+, can be directly determined. The chemical compositions of ambient aerosols are much more complicated. It is found that, besides major ions (e.g. Na^+, K^+, Ca^+, Fe^+, Cl^-, CN^-, NO_3^- and HSO_4^-), C_xH_y, $C_xH_yO_z$ and CNO^- can be identified. With this method, HR-SPAMS can also determine the time series of organic and inorganic peaks, whose m/z are very close to each other (e.g. $41K^+$ with the theoretical m/z value at 40.96182 and $C_3H_5^+$ with the theoretical m/z value at 41.03913). Important organic ion peaks, such as tracer peaks for secondary organic matter like 139[$C_2H_3O_5S^-$] and 153[$C_3H_5O_5S^-$], can be identified. More importantly, our ART-2a classification from HR-SPAMS dataset clearly showed a particle type containing heavy metals like Pb^+, which was obviously ignored in the ART-2a classification from the LR-

SPAMS dataset. More particle types were generated by the ART-2a classification of HR-SPAMS data compared to that of LR-SPAMS data, as the original biomass burning particle type can be divided into three more detailed types based on the different signals of 26[CN^-], 42[CNO^-], 46[NO_2^-] and other organic species like C_xH_y and $C_xH_yO_z$, implying different aerosol aging processes or burning conditions. Such detailed information may be critical to study the aging processes and source appointment of atmospheric aerosols. There is a deficiency of this HR-SPAMS calibration method, which has been showed that some fraction of particles cannot be calibrated due to the presence of weak signals of the marker ions. It can be mitigated by applying some additional marker ions. All the automatic linear calibration method codes specific for HR-SPAMS are open access and can be found at https://github.com/zhuxiaoqiang- fdu/zhuxiaoqiang-fdu. And we proposed the principle of this calibration method can be adopted in other aerosol mass spectrometers.

Author Contribution

Y.X and X.W. supervised this study. X.W. and S.Z. designed the calibration and data analysis methods. S. Wang. and S.Z. performance the sea spray aerosol and ambient aerosol experiment. S.Z. wrote the open source code for calibration and data analysis of the single particle mass spectra and made the GUI program with suggestions from X.W. and X.Y.. X.W. and S.Z. prepared the manuscript with contributions from all co-authors.

Acknowledgments

This work was partially supported by the National Natural Science Foundation of China (Nos. 41827804, 41775150, 21906024, 91544224) and Shanghai Natural Science Foundation (No. 19ZR1404000). The authors thank Hexin Analytical Instrument Co., Ltd., China for providing HR-SPAMS.

Competing interests

The authors declare that they have no conflict of interest.

Reference

Ackerman, A. S., Kirkpatrick, M. P., Stevens, D. E., and Toon, O. B.: The impact of humidity above stratiform clouds on indirect aerosol climate forcing, Nature, 432, 1014-1017, 2004.

Bertram, T. H., Cochran, R. E., Grassian, V. H., and Stone, E. A.: Sea spray aerosol chemical composition: elemental and molecular mimics for laboratory studies of heterogeneous and multiphase reactions, Chemical Society Reviews, 2018. 10.1039.C1037CS00008A, 2018.

Bi, X., Zhang, G., Li, L., Wang, X., Li, M., Sheng, G., Fu, J., and Zhou, Z.: Mixing state of biomass burning particles by single particle aerosol mass spectrometer in the urban area of PRD, China, Atmospheric Environment, 45, 3447-3453, 2011.

Chudinov, A., Li, L., Zhou, Z., Huang, Z., Gao, W., Yu, J., Nikiforov, S., Pikhtelev, A., Bukharina, A., and Kozlovskiy, V.: Improvement of peaks identification and dynamic range for bi-polar Single Particle Mass Spectrometer, International Journal of Mass Spectrometry, 436, 7-17, 2019.

Collins, D. B., Zhao, D. F., Ruppel, M. J., Laskina, O., Grandquist, J. R., Modini, R. L., Stokes, M. D., Russell, L. M., Bertram, T. H., and Grassian, V. H.: Direct aerosol chemical composition measurements to evaluate the physicochemical differences between controlled sea spray aerosol generation schemes, Atmospheric Measurement Techniques Discussions, 7, 6457-6499, 2014.

Dall'Osto and Harrison, M.: Urban organic aerosols measured by single particle mass spectrometry in the megacity of London, ATMOSPHERIC CHEMISTRY and PHYSICS, 12, 2012.

Das, R., Bin Mohamed Mohtar, A. T., Rakshit, D., Shome, D., and Wang, X.: Sources of atmospheric lead (Pb) in and around an Indian megacity, Atmospheric Environment, 193, 57-65, 2018.

Hudson, P. K., Murphy, D. M., Cziczo, D. J., Thomson, D. S., Gouw, J. A. D., Warneke, C., Holloway, J., Jost, H. J., and Hübler, G.: Biomass - burning particle measurements: Characteristic composition and chemical processing, Journal of Geophysical Research Atmospheres, 109, 2004.

Li, L., Liu, L., Xu, L., Li, M., Li, X., Gao, W., Huang, Z., and Cheng, P.: Improvement in the Mass Resolution of Single Particle Mass Spectrometry Using Delayed Ion Extraction, Journal of the American Society for Mass Spectrometry, 29, 2105-2109, 2018.

Luo, J., Zhang, J., Huang, X., Liu, Q., Luo, B., Zhang, W., Rao, Z., and Yu, Y.: Characteristics, evolution, and regional differences of biomass burning particles in the Sichuan Basin, China, Journal of Environmental Sciences, 89, 35-46, 2020.

Ma, L., Li, M., Huang, Z., Li, L., Gao, W., Nian, H., Zou, L., Fu, Z., Gao, J., Chai, F., and Zhou, Z.: Real time analysis of lead-containing atmospheric particles in Beijing during springtime by single particle aerosol mass spectrometry, Chemosphere, 154, 454-462, 2016.

Manuel, D. O., Harrison, R. M., Beddows, D. C. S., Freney, E. J., Heal, M. R., and Donovan, R. J.: Single-particle detection efficiencies of aerosol time-of-flight mass spectrometry during the North Atlantic marine boundary layer experiment, Environmental Science Technology, 40, 5029-5035, 2006.

Moffet, R. C. and Prather, K. A.: In-situ measurements of the mixing state and optical properties of soot with implications for radiative forcing estimates, Proceedings of the National Academy of Sciences of the United States of America, 106, 11872-11877, 2009.

Murphy, D. M.: The design of single particle laser mass spectrometers, Mass Spectrometry Reviews, 26, 150-165, 2010.

Nash, D. G., Baer, T., and Johnston, M. V.: Aerosol mass spectrometry: An introductory review, International Journal of Mass Spectrometry, 258, 2-12, 2006.

Peng, M., Zhao, C., Ma, H., Yang, Z., Yang, K., Liu, F., Li, K., Yang, Z., Tang, S., Guo, F., Liu, X., and Cheng, H.: Heavy metal and Pb isotopic compositions of soil and maize from a major agricultural area in Northeast China: Contamination assessment and source apportionment, Journal of Geochemical Exploration, 208, 106403, 2020.

Pratt, K. A. and Prather, K. A.: Mass spectrometry of atmospheric aerosols-Recent developments and applications. Part II: On-line mass spectrometry techniques, Mass Spectrometry Reviews, 31, 17-48, 2012.

Qin, X., Bhave, P. V., and Prather, K. A.: Comparison of Two Methods for Obtaining Quantitative Mass Concentrations from Aerosol Time-of-Flight Mass Spectrometry Measurements, Analytical Chemistry, 78, 6169-6178, 2006.

Reinard, M. S., Adou, K., Martini, J. M., and Johnston, M. V.: Source characterization and identification by real-time single particle mass spectrometry, Atmospheric Environment, 41, 9397-9409, 2007.

Sodeman, D. A., Toner, S. M., and Prather, K. A.: Determination of Single ParticleMass Spectral Signatures fromLight-Duty Vehicle Emissions, Environmental Science & Technology, 39, 4569-4580, 2005.

Song, X.-H., Hopke, P. K., Fergenson, D. P., and Prather, K. A.: Classification of Single Particles Analyzed by ATOFMS Using an Artificial Neural Network, ART-2A, Analytical Chemistry, 71, 860-865, 1999.

SULLIVAN, R. C. and PRATHER, K. A.: Investigations of the Diurnal Cycle and Mixing State of Oxalic Acid in Individual Particles in Asian Aerosol Outflow, Environmental Science & Technology, 41, p.8062-8069, 2007.

Sullivan, R. C. and Prather, K. A.: Recent advances in our understanding of atmospheric chemistry and climate made possible by on-line aerosol analysis instrumentation, Analytical Chemistry, 77, 3861-3885, 2005.

Surratt, J. D., Chan, A. W. H., Eddingsaas, N. C., Chan, M. N., Loza, C. L., Kwan, A. J., Hersey, S. P., Flagan, R. C., Wennberg, P. O., and Seinfeld, J. H.: Reactive intermediates revealed in secondary organic aerosol formation from isoprene, Proceedings of the National Academy of Sciences of the United States of America, 107, p.6640-6645, 2010.

Surratt, J. D., Kroll, J. H., Kleindienst, T. E., Edney, E. O., Claeys, M., Sorooshian, A., Ng, N. L., Offenberg, J. H., Lewandowski, M., and Jaoui, M.: Evidence for organosulfates in secondary organic aerosol, Environmental Science & Technology, 41, p. 517-527, 2007.

Tsunogai, S., Saito, O., Yamada, K., and Nakaya, S.: Chemical composition of oceanic aerosol, Journal of Geophysical Research, 77, 5283-5292, 1972.

Wang, H., An, J., Shen, L., Zhu, B., Xia, L., Duan, Q., and Zou, J.: Mixing state of ambient aerosols in Nanjing city by single particle mass spectrometry, Atmospheric Environment, 132, 123-132, 2016.

Wang, H., Shen, L., Yin, Y., Chen, K., Chen, J., and Wang, Y.: Characteristics and mixing state of aerosol at the summit of Mount Tai (1534 m) in Central East China: First measurements with SPAMS, Atmospheric Environment, 213, 273-284, 2019.

Wenzel, R. J., Liu, D. Y., Edgerton, E. S., and Prather., K. A.: Aerosol time - of - flight mass spectrometry during the Atlanta Supersite Experiment: 2. Scaling procedures, Journal of Geophysical Research:

476 Atmospheres, 2003. 2003.

477 Zelenyuk, A. and Imre, D.: Beyond single particle mass spectrometry: multidimensional
478 characterisation of individual aerosol particles, International Reviews in Physical Chemistry, 28, 309-
479 358, 2009.

480 Zhang, G., Bi, X., Chan, L. Y., Wang, X., Sheng, G., and Fu, J.: Size-segregated chemical characteristics of
481 aerosol during haze in an urban area of the Pearl River Delta region, China, Urban Climate, 4, 74-84,
482 2013.

483 Zhang, R. J. and Kin-Fai, H. O.: The Role of Aerosol in Climate Change,the Environment,and Human
484 Health, Atmospheric Oceanic Science Letters, 5, 156-161, 2012.
485

486

487

488

489

490

Figure Captions

Figure 1. The GUI program for HR-SPAMS calibration

Figure 2. Linear calibration with reference ion peaks

Figure 3. Probability distributions of the marker peak locations before and after Automatic Linear Calibration (AL-Cal) for (a) sea spray aerosol and (b) ambient aerosol

Figure 4. Averaged positive and negative mass spectra of sea spray aerosols

Figure 5. Averaged positive and negative mass spectra of ambient aerosols

Figure 6. Time series of peak intensities at m/z 40.95 and m/z 41.01

501 Table 1. Possible peak assignments for the m/z of reference ions for sea spray aerosol and
502 ambient aerosol

Unit mass resolution m/z	Possible species (Sea spray aerosol)	Unit mass resolution m/z	Possible species (Ambient aerosol)
+24	Mg^+ C_2^+	+39	K^+ $C_3H_3^+$
+39	K^+ $C_3H_3^+$	+56	Fe^+ Si_2^+ CaO^+ KOH^+
+81	Na_2Cl^+ Br^+ $C_6H_9^+$	-26	CN^- BO^- $C_2H_2^-$
+113	K_2Cl^+ $C_9H_5^+$	-62	NO_3^- $C_5H_2^-$
+115	K_2Cl^+ $C_9H_7^+$	-96	SO_4^- $BrOH^-$
-26	CN^- BO^- $C_2H_2^-$	-97	HSO_4^- C_8H^- BrO^- $NaCl_2^-$ $H_2PO_4^-$
-37	Cl^- C_3H^-		
-42	BO_2^- CNO^-		
-129	$MgCl_3^-$ $C_{10}H_9^-$ $(C_3H_7)_2C_2H_5^-$ $CaCl_2OH^-$		
-131	$MgCl_3^-$		

503
504
505
506
507
508
509

Table 2. Peak identification of important chemical species in sea spray aerosols. The first column is the measured m/z for peaks. The second and third columns shows the theoretical m/z bin value and theoretical m/z value of most possible species for each peak

Measurement m/z(positive)	Possible species (theoretical m/z bin value)	Possible species (theoretical m/z value)	Measurement m/z(negative)	Possible species (theoretical m/z bin value)	Possible species (theoretical m/z value)
22.993	Na^+(22.993)	Na^+(22.98977)	15.0344	CH_3^-(15.0216)	CH_3^-(15.02348)
23.9829	Mg^+(23.9829)	Mg^+(23.98505)	34.9641	Cl^-(34.9641)	Cl^-(34.96885)
27.0267	$C_2H_3^+$(27.0267)	$C_2H_3^+$(27.02348)	41.9864	CNO^-(41.9971)	CNO^-(41.99799)
38.9672	K^+(38.9672)	K^+(38.96371)	25.0163	C_2H^-(25.0081)	C_2H^-(25.00783)
39.9711	Ca^+(39.9607)	Ca^+(39.96259)	38.0024	$C_3H_2^-$(38.0126)	$C_3H_2^-$(38.01565)
43.9614	CS^+(43.9723)	CS^+(43.9721)	44.9883	HCO_2^-(44.9994)	HCO_2^-(44.99767)
45.983	Na_2^+(45.983)	Na_2^+(45.97954)	49.002	C_4H^-(49.0135)	C_4H^-(49.00783)
59.9569	SiO_2^+(59.9696)	SiO_2^+(59.96677)	57.9574	$NaCl^-$(57.9574)	$NaCl^-$(57.95865)
71.9872	C_6^+(72.0012)	C_6^+(72)			
80.9438	Na_2Cl^+(80.9438)	Na_2Cl^+(80.94839)	63.9574	SO_2^-(63.9574)	SO_2^-(63.96191)
112.898	K_2Cl^+(112.898)	K_2Cl^+(112.89627)	75.9498	SiO_3^-(75.9642)	SiO_3^-(75.96196)
138.89	$Na_3Cl_2^+$(138.907)	$Na_3Cl_2^+$(138.90702)			
140.897	$Na_3Cl_2^+$(140.897)	$Na_3Cl_2^+$(140.90407)	79.9547	SO_3^-(79.9547)	SO_3^-(79.95683)
			80.9015	Br^-(80.9164)	Br^-(80.91629)
			85.9484	$NaPO_2^-$(85.9484)	$NaPO_2^-$(85.95337)
			99.9499	$CaCO_3^-$(99.9499)	$CaCO_3^-$ (99.94735)
			109.917	$CaCl_2^-$(109.9)	$CaCl_2^-$(109.9003)
			128.901	$MgCl_3^-$(128.883)	$MgCl_3^-$ (128.89161)

Table 3. Peak identification of important chemical species in ambient aerosols. The first column is the measured m/z for each peak. The second and third columns shows the theoretical m/z bin value and theoretical m/z value of most possible specie for each peak

Measurement m/z(positive)	Possible species(theoretical m/z bin value)	Possible species(theoretical m/z value)	Measurement m/z(negative)	Possible species(theoretical m/z bin value)	Possible species(theoretical m/z value)
22.993	Na^+(22.993)	Na^+(22.98977)	15.0408	CH_3^-(15.0216)	CH_3^-(15.02348)
23.9991	C_2^+(23.9991)	C_2^+(24)	16.0091	O^-(15.9959)	O^-(15.99492)
25.002	C_2H^+(25.0103)	C_2H^+(25.00783)	17.0145	OH^-(17.0009)	OH^-(17.00275)
26.0087	$C_2H_2^+$(26.0171)	$C_2H_2^+$(26.01565)	26.0078	CN^-(25.9994)	CN^-(26.00307)
30.0171	NO^+(29.999)	NO^+(29.99799)	31.987	O_2^-(31.987)	O_2^-(31.98984)
35.9925	C_3^+(36.0023)	C_3^+(36)	34.9641	Cl^-(34.9641)	Cl^-(34.96885)
36.9976	C_3H^+(37.0076)	C_3H^+(37.00783)	41.9971	CNO^-(41.9971)	CNO^-(41.99799)
38.0065	$C_3H_2^+$(38.0166)	$C_3H_2^+$(38.01565)	45.9897	NO_2^-(45.9897)	NO_2^-(45.99291)
38.9672	K^+(38.9672)	K^+(38.96371)	47.9911	C_4^-(47.993)	C_4^-(48)
47.993	C_4^+(47.993)	C_4^+(48)	61.9808	NO_3^-(61.9938)	NO_3^-(61.98783)
48.9911	C_4H^+(49.0026)	C_4H^+(49.00783)	71.0014	$C_3H_3O_2^-$(71.0153)	$C_3H_3O_2^-$ (71.01332)
49.9994	$C_4H_2^+$(50.0111)	$C_4H_2^+$(50.01565)	78.9548	PO_3^-(78.9548)	PO_3^-(78.95852)
55.9443	Fe^+(55.932)	Fe^+(55.93494)	79.94	SO_3^-(79.9547)	SO_3^-(79.95683)
59.9951	C_5^+(59.9951)	C_5^+(60)	80.946	HSO_3^-(80.9609)	HSO_3^-(80.96466)
60.9946	C_5H^+(61.0074)	C_5H^+(61.00783)	95.9825	SO_4^-(95.9502)	SO_4^-(95.95175)
62.0023	$C_5H_2^+$(62.0152)	$C_5H_2^+$(62.01565)	96.9546	HSO_4^-(96.9546)	HSO_4^-(96.95958)
72.0012	C_6^+(72.0012)	C_6^+(72)	121.01	$C_{10}H^-$(121.01)	$C_{10}H^-$(121.00783)
84.0108	C_7^+(83.9957)	C_7^+(84)	122.01	$C_{10}H_2^-$(122.01)	$C_{10}H_2^-$ (122.01565)
207.976	Pb^+(207.967)	Pb^+(207.97664)	134.008	$C_{11}H_2^-$(134.008)	$C_{11}H_2^-$ (134.01565)

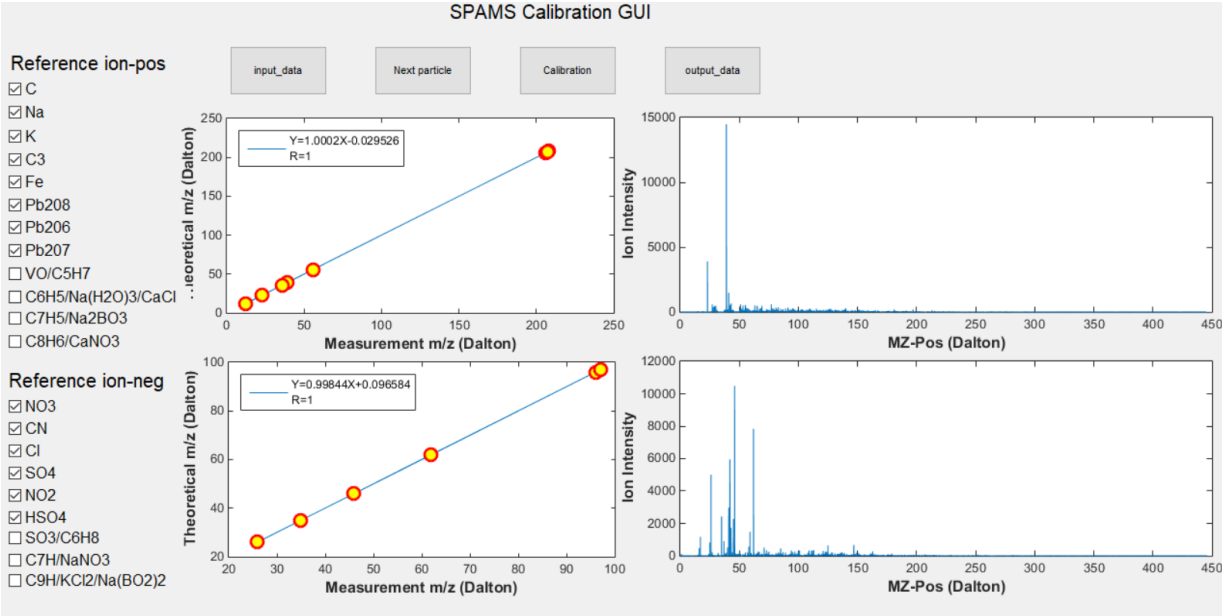

Figure 1. The GUI program for HR-SPAMS calibration

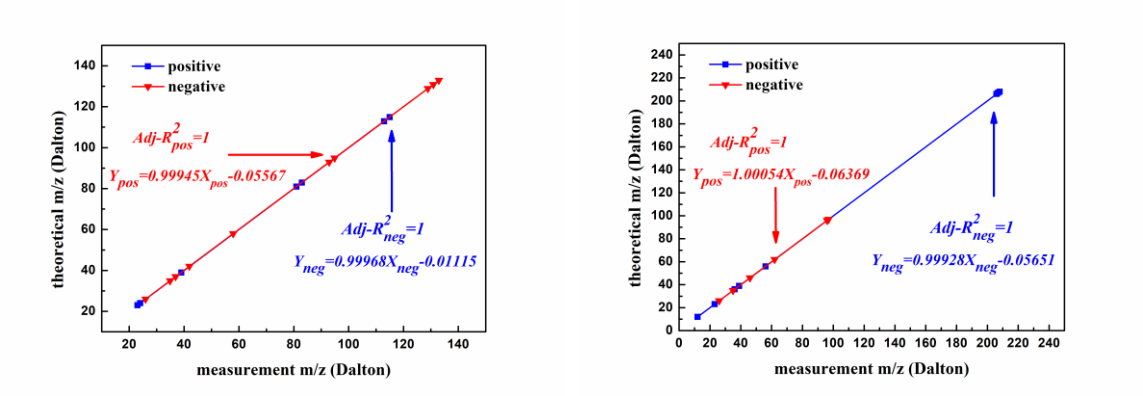

(a)sea spray aerosol (b)ambient aerosol

Figure 2. Linear calibration with reference ion peaks

548 a.

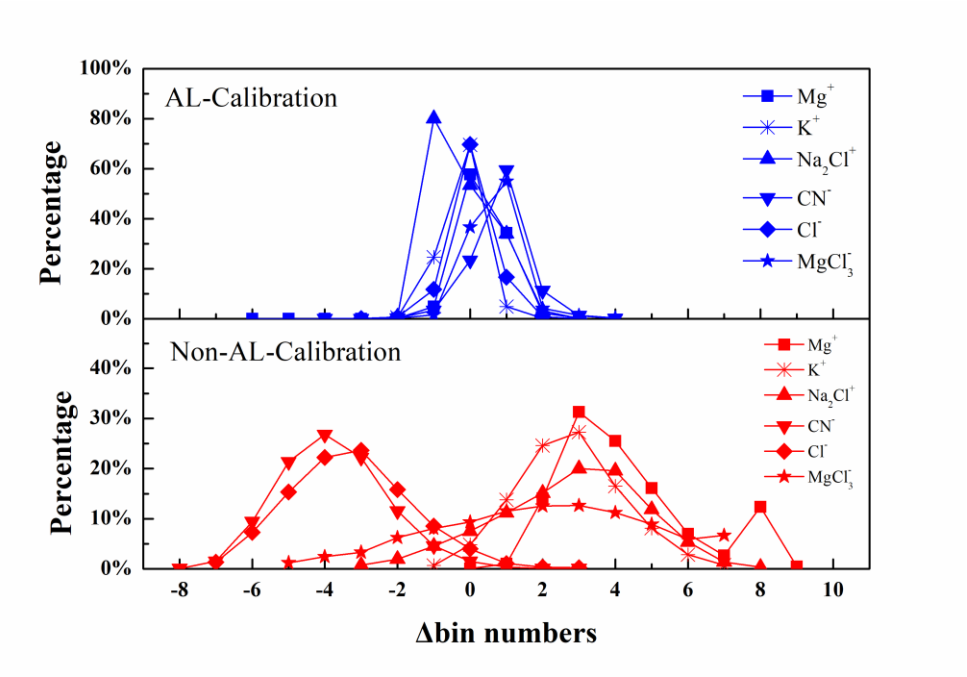

549

550 b.

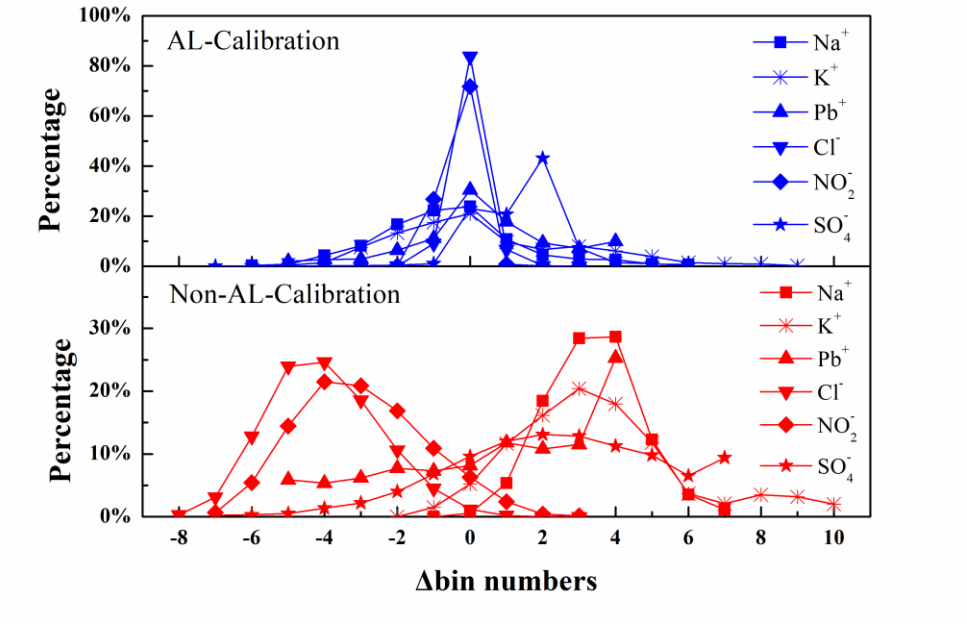

551

552 Figure 3. Probability distributions of the marker peak locations before and after Automatic
553 Linear Calibration (AL-Cal) for (a) sea spray aerosol and (b) ambient aerosol

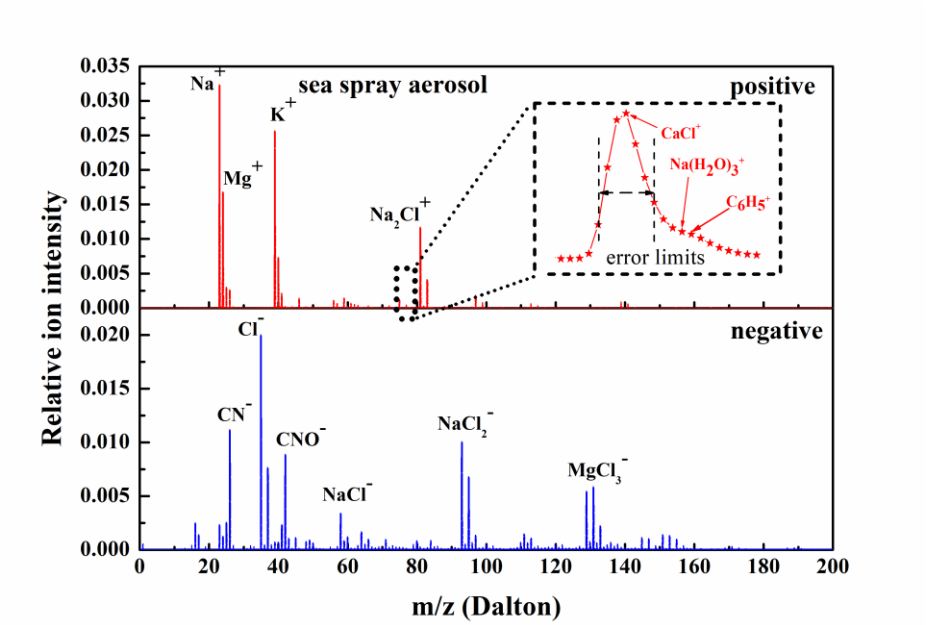

Figure 4. Averaged positive and negative mass spectra of sea spray aerosols

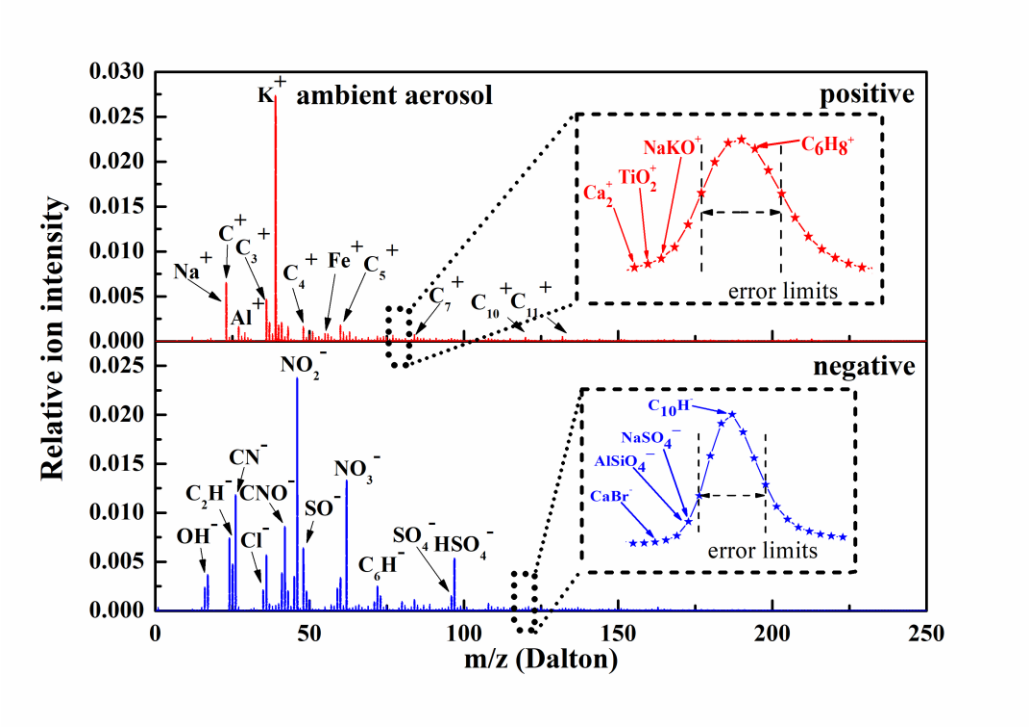

Figure 5. Averaged positive and negative mass spectra of ambient aerosols

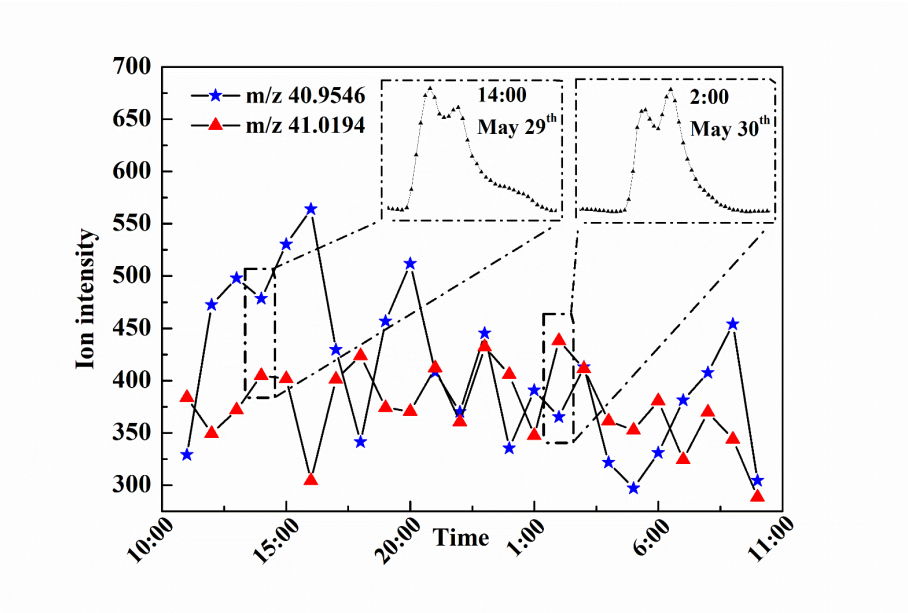

Figure 6. Time series of peak intensities at m/z 40.95 and m/z 41.01